Magnetic Stars, 2011, pp. 188 – 198

Magnetic Field in X–Ray Binary Cygnus X–1

Karitskaya E. A.[1], **Bochkarev N. G.**[2], **Hubrig S.**[3], **Gnedin Yu. N.**[4], **Pogodin M. A.**[4], **Yudin R. V.**[4], **Agafonov M. I.**[5], **Sharova O. I.**[5]

[1] Institute of Astronomy RAS, Moscow, Russia
[2] Sternberg Astronomical Institute, Moscow, Russia
[3] Astrophysical Institute Potsdam, Potsdam, Germany
[4] Central Astronomical Observatory at Pulkovo, Saint–Petersburg, Russia
[5] Radiophysical Research Institute (NIRFI), Nizhny Novgorod, Russia

Abstract. Our spectroscopic observations with FORS1 at the 8.2–m VLT telescope (Paranal, Chile) lead to detection of a magnetic field in the X–ray binary Cyg X–1. That is the first successful attempt of measuring the magnetic field in a binary with a black hole. The value of the mean longitudinal magnetic field in the optical component (O9.7 Iab supergiant) changes regularly with the orbital phase reaching its maximum of 130 G ($\sigma \approx 20$ G). The measurements based on the Zeeman effect were carried through over all the observed supergiant photosphere absorption spectral lines. Similar measurements over the emission line He II λ4686 Å yielded a value of several hundreds Gauss of a smaller significance level. The system Doppler tomogram we have built over the line profiles shows that He II λ4686 Å originates in the outer regions of the accretion structure. The values measured correspond, in the frame of the disc accretion standard model, to a near–black–hole field of $\sim 10^8 - 10^9$ G and may be responsible for the observed Cyg X–1 X–ray flickering. Also some consequences of existence of such a magnetic field in Cyg X–1 optical component's photosphere were suggested.

Key words: spectropolarimetry – circular polarization – magnetic field – Cyg X–1 – O–supergiant – black hole – accretion structure – X–ray flickering – Doppler tomography

1 Introduction

Cyg X–1 = V 1357 Cyg = HDE 226868 is an X–ray binary system with the orbital period $P = 5\overset{d}{.}6$, whose relativistic component is the first black hole (BH) candidate. The optical component (O9.7 Iab supergiant) is responsible for about 95 % of the system's optical luminosity. The remaining 5 % are due to the accretion structure (disc and surrounding gas) near the BH. The optical spectrum mostly consists of O–supergiant absorbtion photospheric lines; the accretion structure emission components exist only in He II 4686 Å and Hα profiles; stellar wind P Cyg components are present in H and He I lines as well as in some O II lines (Karitskaya et al., 2008). The stellar wind is $\dot{M} \sim (2-3)\cdot 10^{-6} M_\odot$/yr (Gies et al., 2003). The chemical peculiarities were found in the O9.7 Iab supergiant photosphere. The Cyg X–1 supergiant atmosphere shows high excesses of He, N, Ne, Mg, Si (the elements by CNO and α–processes) on a factor of 2.5 – 8 (see Karitskaya, 2007; Karitskaya et al., 2007b; Karitskaya et al., 2011). It looks like the mixing of matter in all probability is due to tidal interactions and mass exchange with the relativistic component at the preceding and present stages of evolution.

Both linear and circular polarizations were detected in Cyg X–1 optical continuum and investigated in the 1970s. Linear interstellar and circumstellar polarization reaches the value of $\sim 5\,\%$ (Kemp et al., 1976). Its strength and position angle vary on the scale of years (Nagae et al., 2009). Kemp (1980) detected a component of an amplitude $\sim 0.25\,\%$ which is variable over the orbital phase φ. This component shows a complicated and variable dependence from φ. Similar behavior was found for the circular polarization discovered by Shulov & Kopatskaya (1972), Gehrels (1972). Interstellar circular polarization does not exceed $0.04\,\%$, and in the variable component with the period of $2.8/5.6^d$ it is about $0.02\,\%$ (Michalsky and Swedlung, 1977). While the intrinsic circular polarization is most probably generated by a magnetic field, the intrinsic linear polarization in Cyg X–1 is usually explained by electron scattering on non–symmetrical gas structures (e. g. Bochkarev et al., 1979; Karitskaya, 1981; Bochkarev et al., 1986; Dolan and Tapia, 1989).

The X–ray binary Cyg X–1 is a microquasar. Theoretical models describing processes in objects with black holes, like microquasars or active galactic nuclei, are dominated by the magnetic–disk–accretion paradigm. Nevertheless, no reliable measurements of magnetic fields in these systems were available so far. Shvartsman (1971) was the first to predict the existence of a magnetic field in Cyg X–1 . He wrote that the flickering X–ray emission from Cyg X–1 points at the presence of a black hole and indicated the role of the magnetic field in the accretion onto a black hole (Pustilnik and Shvartsman, 1974; Kaplan and Shvartsman, 1976). Theoretical estimations of the strength of the magnetic field in Cyg X–1 were based on optical polarization (Dolginov et al., 1995; Gnedin et al., 2005). The upper limits $B < 350\,\mathrm{G}$ for the optical component and $B \lesssim 500\,\mathrm{G}$ for the outer part of the accretion disc were found. There were many attempts to search for the magnetic field of the optical component of the Cyg X–1 binary (the O9.7 Iab supergiant), but all these efforts resulted in upper limits only. For example, spectropolarimetric observations of Zeeman effect with the 6–m BTA telescope (Gnedin et al., 2003) in He II $\lambda 4686\,$Å line yielded the upper limit $B < 1000\,\mathrm{G}$ for the region of the line emission. Our spectropolarimetric observations on the VLT were the first successful attempt of measuring the magnetic field in a binary with a black hole.

2 Observations, Method and Reduction

Our spectropolarimetric observations were performed with the 8.2–m Very Large Telescope (VLT) of the European Southern Observatory (Cerro Paranal, Chile) in its service mode with the FORS1 spectrograph in June/July, 2007 and in July, 2008 (Table 1). The spectra were obtained in the $3680-5129\,$Å spectral range with the spectral resolution of $R = 4000$ and the signal–to–noise ratio $S/N = 1500-3500$ for spectra of intensity (Stokes I parameter). Cyg X–1 was in its X–ray "hard state" at that time. 13 spectropolarimetric spectra (for both Stokes parameters I and V) with exposure times of ~ 1 hour were obtained during 13 nights. We obtained 6 spectra over June 18 – July 9, 2007 and 7 spectra over July 14 – July 30, 2008. Each observation included 8 exposures 500 s each.

The details on the observing technique with the FORS1 and data reduction can be found, for example, in Hubrig (2004); also see references therein. Using the method described there (the least squares technique, hereinafter LST), we obtained the mean longitudinal magnetic field $\langle B_z \rangle$; it is the magnetic field component along the line of sight, averaged over the visible stellar hemisphere and weighted by the local emergent spectral line intensity. It is diagnosed from the slope of the linear regression of V/I versus $-\frac{g_{\rm eff}\, e}{4\pi m_e c^2}\lambda^2 \frac{1}{I}\frac{\mathrm{d}I}{\mathrm{d}\lambda}\,\langle B_z\rangle + V_0/I_0$, where V is the Stokes parameter measuring the circular polarization, I — the intensity observed in unpolarized light, $g_{\rm eff}$ — the effective Landé factor, e — the electron charge, λ — the wavelength, m_e — the electron mass, c — the speed of light, $\mathrm{d}I/\mathrm{d}\lambda$ — the derivative of the Stokes I parameter, V_0/I_0 — a constant, and $\langle B_z \rangle$ is the mean longitudinal field. The method is statistical: to increase the sensitivity, we used all the observed spectral lines simultaneously. For our observations we adopt the effective Landé factor $g_{\rm eff} = 1.07$

Table 1: Magnetic field from the VLT spectropolarimetric observations of the X–ray binary Cyg X–1

Date	JD*	Orbital phase	$\langle B_z \rangle$, G	σ, G	significance $\lvert \langle B_z \rangle / \sigma \rvert$
18–19 June 2007	2454270.768	0.650	−6	28	0.2
19–20 June 2007	2454271.778	0.830	37	22	1.7
20–21 June 2007	2454272.760	0.006	58	21	2.8
25–26 June 2007	2454277.808	0.907	22	28	0.8
29–30 June 2007	2454281.707	0.603	48	20	2.4
9–10 July 2007	2454291.766	0.400	101	18	5.5
14–15 July 2008	2454662.711	0.641	49	23	2.1
15–16 July 2008	2454663.684	0.816	22	22	1.0
16–17 July 2008	2454664.692	0.995	80	23	3.5
17–18 July 2008	2454665.692	0.174	24	19	1.3
23–24 July 2008	2454671.704	0.247	−16	20	0.8
24–25 July 2008	2454672.728	0.430	27	19	1.4
30–31 July 2008	2454678.676	0.500	128	21	6.2

* JD is the Julian date of the middle of observation; orbital phases φ are according to the ephemeris from Brocksopp et al. (1999): $\varphi = 0$ corresponds to the optical component in front; σ is the standard deviation.

according Hubrig et al. (2008).

The method used has been already applied (and carefully tested) in previous studies of bright magnetic stars (Hubrig et al., 2004; Bagnulo et al., 2002; Bagnulo et al., 2006) which usually do not have significant interstellar or intrinsic linear polarization and have rather strong $\langle B_z \rangle = 500 - 2000$ G. By contrast, Cyg X–1 has $\langle B_z \rangle$ weaker and a strong interstellar/circumstellar linear polarization. For this reason we had to meet some precautions in the magnetic field measurements of this system and adapt the method for such conditions. For more details please see the paper by Bochkarev & Karitskaya (2011) in this edition.

We removed all spectral features not belonging to the photosphere of the Cyg X–1 optical component (O9.7 Iab): interstellar lines, CCD flaws, the He II $\lambda 4686$ Å emission line, lines with strong P Cyg components. Telluric lines being rather weak in the considered spectral range, we find no pollution from these lines in our low–resolution spectra.

Before applying the procedures for the magnetic field measurements, we removed the linear trends from our V/I–continua, most probably caused by the crosstalk between linear and circular polarization within the FORS1 (Bochkarev & Karitskaya, 2011). This seems to be an appropriate step, since as follows from Nagae et al. (2009), the optical–range linear polarization of Cyg X–1 has no significant spectral line features. Therefore, according to our estimates, the crosstalk can produce only a false V continuum slope and does not significantly distort the S–shaped V profiles of the spectral lines caused by the Zeeman effect (hereafter, Zeeman S–waves). The Stokes I spectra were normalized to the pseudo–continuum I_c, which is produced by the source energy distribution, interstellar reddening, broad diffuse interstellar bands (DIBs), as well as atmospheric extinction and detector sensitivity. After these reductions, the residual deviations of the least–squares linear regression follow the Gauss function up to $\pm 3.6\,\sigma(V/I)$, where $\sigma(V/I)$ is the standard deviation of V/I, i. e. the level of significance corresponds to the Gauss statistics now.

To verify our results (see Table 1), we made several tests: (1) each spectrum was subdivided in two halves at mid–wavelength to check that $\langle B_z \rangle$ values determined over each half separately were in agreement within error bars. (2) We repeated $\langle B_z \rangle$ calculations using the fragments of spectra that include strong absorption lines (deeper than 4 %) only: $\sim 1/3$ spectral points were used and

$\langle B_z \rangle$ values were found in agreement with our earlier measurements using the whole spectral range within $1.5\,\sigma(\langle B_z \rangle)$. (3) Zeeman S–waves were found for the strongest lines. In Fig. 2a we show an example of a distinct Zeeman feature for the line He I λ4026 Å.

We should note that the element overabundance on the order of 2.5 – 8 in the Cyg X–1 optical component's stellar atmosphere (Karitskaya, 2007; Karitskaya et al., 2007b; Karitskaya et al., 2011) enforces the spectral lines and Zeeman S–waves. It increases the accuracy of $\langle B_z \rangle$ measurements.

3 Cyg X-1 Supergiant's Atmospheric Magnetic Field

The results of our measurements of $\langle B_z \rangle$ at different orbital phases, φ, are presented in Table 1 and Fig. 1. Figure 1 shows the mean longitudinal magnetic field of the Cyg X–1 optical component $\langle B_z \rangle$ versus the orbital phase φ for 2007, for 2008, and for 2007 and 2008 together. The error bars are 68 % confidence intervals. The phases of orbital period of 5.6 days were calculated with the ephemerides by Brocksopp et al. (1999), $\varphi = 0$ corresponds to the moment, when the BH component is located behind the optical component (O9.7 Iab supergiant).

The magnetic field was detected at a high confidence level (about $6\,\sigma$) near the orbital phases $\varphi = 0.4$ in 2007, and $\varphi = 0.5$ in 2008. It follows from Fig. 1c that $\langle B_z \rangle$ varies periodically with the orbital phase (two waves for period), reaching 130 G ($\sigma \cong 20$ G) at the phase 0.5. The power spectrum formally produced by Deeming's method is in agreement with the one–half orbital period. The dependence of $\langle B_z \rangle$ on φ is more complicated than that for the magnetic dipole and has probably changed from 2007 to 2008.

4 Magnetic Field on the Outer Part of the Accretion Structure

4.1 He II λ4686 Å Spectral Line Investigation

As the next step of our study, we investigated the He II λ4686 Å spectral line separately. Due to the presence of a strong emission component in the line profile, it was omitted from the earlier analysis. In fact, this line has a compound profile consisting of absorption (originating in the stellar photosphere) and emission (originating in the accretion structure) components. Certainly, the accuracy of the magnetic field measurements using just a single line is considerably worse compared to those using the whole spectrum. Nevertheless, our analysis shows the results for the two spectra at the $4\,\sigma$ level: $\langle B_z \rangle = -730 \pm 170$ G for the orbital phase $\varphi = 0.65$ in 2007 and $\langle B_z \rangle = -420 \pm 106$ G for $\varphi = 0.43$ in 2008. The Zeeman S–wave in the V–spectrum smoothed over 3 Å and its correspondence to the $\mathrm{d}I/\mathrm{d}\lambda$ wave are presented in Fig. 2b for June 18, 2007.

To exclude the influence of the stellar–photosphere absorption component of He II λ4686 Å, we subtracted the model–atmosphere line profile for each φ. We calculated it using the method described, for example, in Karitskaya et al. (2005) and Karitskaya et al. (2007a). The tidal distortion of the star, the illumination of the atmosphere by the X–ray flux and non–LTE effects for H I, He I, Mg II, Si IV were taken into account in the stellar atmosphere modelling. The values $T_{\rm eff} = 30400 \pm 500$ K, $\log g = 3.31 \pm 0.07$ were used for the calculation of He II λ4686 Å profile. The uncertainties of parameters permit us to vary the theoretical profiles in the admissible limits.

Fig. 3 shows the process we used for theoretical profile subtracting for $\varphi = 0.65$ (June 18, 2007) and 0.91 (June 25, 2007) as examples. The substraction changes the numerical values of $\langle B_z \rangle$ but does not distort the qualitative result: the presence of a magnetic field of the order of $\sim (300-1000)$ G, on a significance level of about $(2.5-3.5)\,\sigma$ in the region of formation of the λ4686 Å emission.

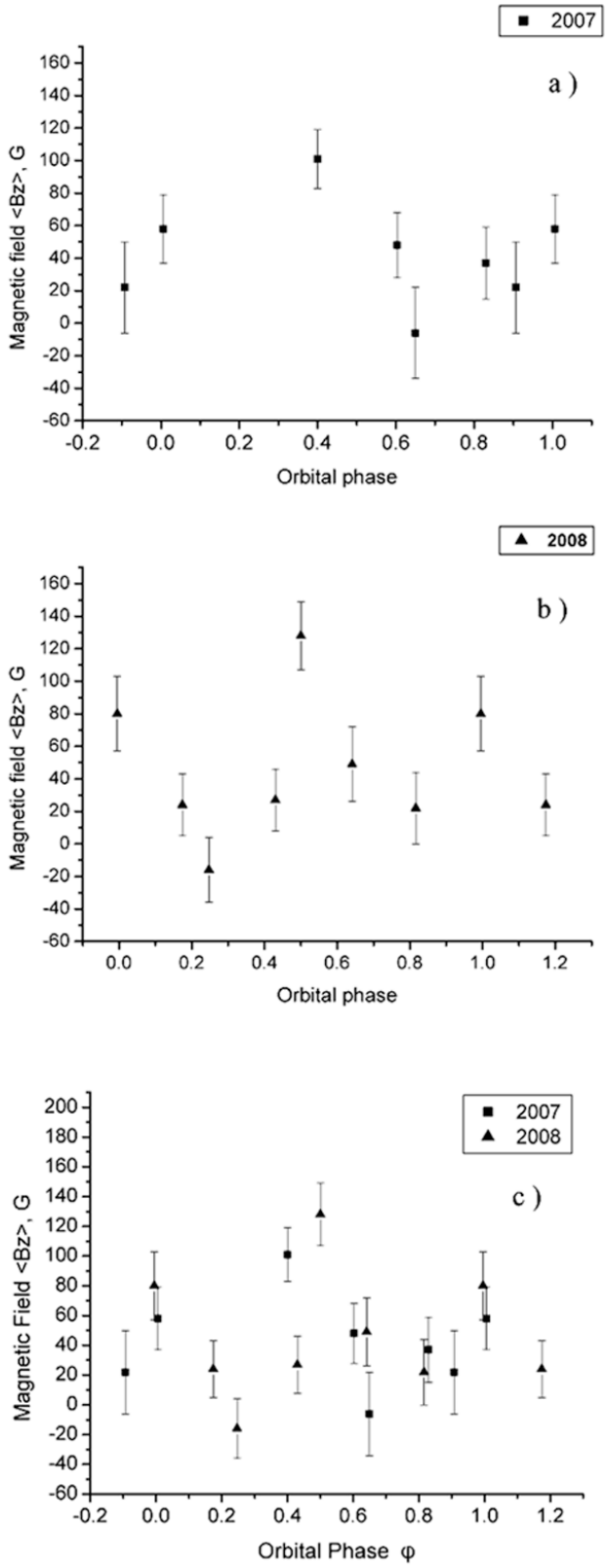

Figure 1: The mean longitudinal magnetic field of the Cyg X–1 optical component $\langle B_z \rangle$ (in Gauss) *vs.* the orbital phase φ for 2007 (a), for 2008 (b), and for both years (c). Full squares indicate the 2007 data, full triangles — the 2008 data. The error bars are 68 % confidence intervals.

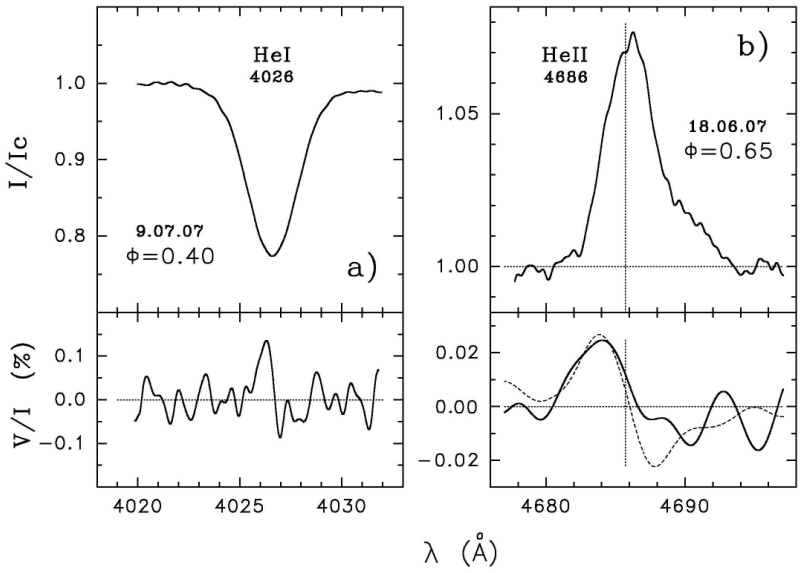

Figure 2: Examples of Zeeman S–waves showing the accordance of wavelength dependence of intensity normalized to the continuum I/I_c to the Zeeman S–waves of V/I spectra are given for Cyg X–1. (a) — an example of Zeeman S–waves for the O–star atmosphere absorption spectral lines: Zeeman S–wave (bottom panel) in the region of He I λ4026 Å line (top) observed July 9, 2007 when $\langle B_z \rangle$ was high (see Table 1). (b) — the He II λ4686 Å spectral line profile I/I_c for June 18, 2007 (top); the solid curve in the bottom panel shows the observed V/I spectrum smoothed over 3 Å. The dashed curve displays the expected Zeeman S–wave shape $(\mathrm{d}I/\mathrm{d}\lambda)/I \propto V/I$, where I is smoothed over 3 Å. A good agreement between these curves demonstrates a possible existence of a rather large magnetic field in the region of forming He II λ4686 Å emission.

4.2 Doppler Tomography in He II λ4686 Å Line

To find the He II λ4686 Å line formation regions we constructed a Doppler tomogram (the binary system image in the velocity space) based on our VLT observational data. We used a new Doppler tomogram reconstruction technique worked out by Agafonov (2004), the so–called Radioastronomical Approach (RA). This RA method includes an effective CLEAN procedure and allows to reconstruct well the 2D velocity field with a very small number of 1D profiles (5 – 10 spectra may be sufficient), see, e.g. Fig. 1 in Agafonov et al. (2006). The tomography map constructed on the basis of all the 13 VLT He II λ4686 Å line profiles obtained by us in 2007 and 2008 is presented in Fig. 4. It shows that He II λ4686 Å line emission regions are located near the L1 point in the Roche lobe model, and near the "hot spot" or "hot line" (Boyarchuk et al., 2002) on the outer part of the accretion structure. The absorption component originates in the O–supergiant photosphere. However, at different observational seasons Cyg X–1 tomogram maps may differ from one another — the matter flow changes on the scale of years (Karitskaya et al., 2005; Karitskaya et al., 2007a). Therefore, we also constructed the tomograms using our VLT profiles separately for the year 2007 and 2008. They show a similar result. The same conclusion about the He II λ4686 Å line formation regions was done in Karitskaya et al. (2005) by using the profiles from the Peak Terskol Observatory Cyg X–1 observations. Consequently, $\langle B_z \rangle$ derived from He II emission line is located in the outer parts of the accretion structure. The values 400 – 800 G are in agreement with the estimation by Gnedin et al. (2005).

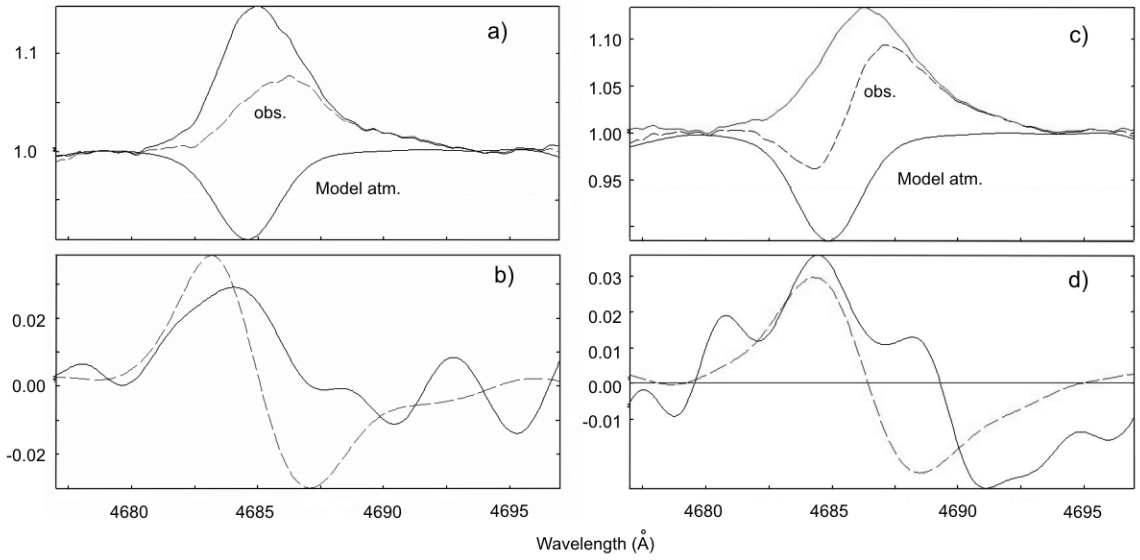

Figure 3: The examples of excluding the influence of the stellar–photosphere absorption component of He II λ4686 Å. (a) — the He II λ4686 Å spectral line profile I/I_c for June 18, 2007, $\varphi = 0.65$ (dashed line denoted as "obs."). The upper solid line is the pure residual emission profile after subtracting the model atmosphere absorption profile originated in the optical star's photosphere (see the curve denoted as "Model atm."). (b) — the solid curve shows the observed V/I spectrum smoothed over 3 Å. The dashed curve displays the expected Zeeman S–wave shape $(\mathrm{d}I/\mathrm{d}\lambda)/I \propto V/I$, where I is smoothed over 3 Å for the residual profile from (a). (c) and (d) show similar curves only for June 25, 2007, $\varphi = 0.91$. The resulted magnetic fields $\langle B_z \rangle$ for this cases are 320 G and 640 G.

5 Consequences and Conclusions

5.1 Possible Magnetic Field Influence on the Matter Flow

We discovered a mean longitudinal magnetic field averaged over the picture plane $\langle B_z \rangle \sim 100$ G in the photosphere of the optical component of Cyg X–1 . The real magnetic field may exceed $\langle B_z \rangle$. Near the magnetic poles it may reach or even exceed 300 G.

Cyg X–1 optical component model atmosphere was computed in Karitskaya et al. (2005) and Karitskaya et al. (2007a). The X–ray illumination by "soft" and "hard" spectra was taken into account. For the calculations we used the supergiant parameters $T_{\rm eff} = 30400 \pm 500$ K, $\log g = 3.31 \pm 0.07$, obtained in the mentioned research by a non–LTE model atmosphere method.

Figure 5 shows the pressure versus optical depth in Cyg X–1 optical component's atmosphere. The common logarithm of Rosseland mean of optical depth $\tau_{\rm R}$ is the abscissa axis. The common logarithm of pressure (the pressure grows in the downward direction) is shown by the ordinate axis. The relation of the sum of gas and radiation pressure on $\tau_{\rm R}$ is shown by the sloped solid line. The sloped dashed line with short intervals between the strokes shows the relation for gas pressure on $\tau_{\rm R}$. The pressure differences between the relations for the X–ray–illuminated and not X–ray–illuminated atmosphere is small — within the line width. The horizontal lines show the magnetic pressure for magnetic strength B equal to 300 G (solid line) and 100 G (dashed line). The star's photosphere is marked by a light–shaded area. The dark–shaded area marks the star's chromosphere with the temperature inversion which appears in the case of the "soft" X–ray state.

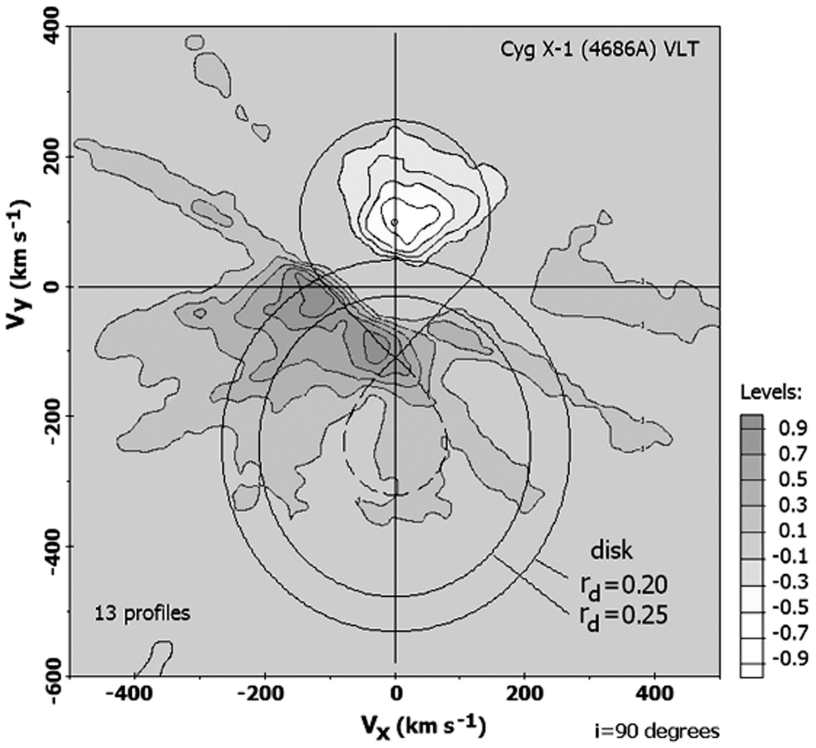

Figure 4: Doppler tomogram of Cyg X–1 in He II λ4686 Å. It is constructed based on 13 VLT spectra from 2007 – 2008, and shows brightness of emission in He II λ4686 Å spectral line on the velocity plane (V_x, V_y). Thin lines are the isophotes of different levels shown on the right part of the figure (in relative units). The zero level corresponds to the "pseudo–continuum"; negative values correspond to absorption, and positive ones — to emission. The dashed line shows the Roche lobe of the black hole (BH). The optical component, almost filling its Roche lobe is drawn by the solid line. The Roche lobes are constructed for the mass ratio $q = M_{\rm X}/M_{\rm O} = 1/3$. Here $M_{\rm X}$ is the mass of the X–ray emitting component (the BH) and $M_{\rm O}$ is the mass of the optical component (the O–star). The ovals represent the outer parts of the accretion disks with radii $r_{\rm d} = 0.2$ and 0.25 of the distance between the centers of mass of the components.

Figure 5 shows that magnetic pressure becomes comparable not only with gas pressure but also with the sum of gas and radiation pressure in the stellar photosphere and may even exceed them near the magnetic poles. Hence, we may expect the magnetic field to influence the matter outflow (the stellar wind), as well as the accretion flow.

The magnetic field was detected at a high confidence level (about $6\,\sigma$) near the orbital phases $\varphi = 0.4$ in 2007, and 0.5 in 2008. We registered the maximum near $\varphi = 0.5$. Therefore, near this phase one of magnetic poles is on the side of the observer and is located not so far from the L1 point. The dependence of $\langle B_z \rangle$ from φ is more complicated than that for the magnetic dipole and probably varies within one year (Fig. 1). The magnetic field structure variability may be the reason of some long–term variations of matter–flow process in this binary system.

Near the magnetic poles, where the magnetic pressure forms a significant part of the full pressure, the gas pressure (and so its density) must be considerably lower then elsewhere. Consequently, at the poles we may pierce deeper inside and see hotter atmospheric layers. Hence we may expect the existence of hot spots with only slight differences in temperature. Such spots may influence the light curve and spectral line profiles.

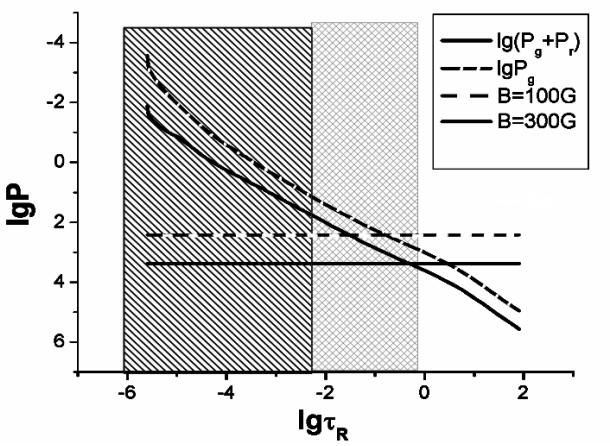

Figure 5: A comparison of gas pressure and the sum of gas and radiation pressure with the magnetic pressure in the atmosphere of Cyg X–1 optical component (the O–supergiant). Shown here is the relation of gas pressure (the dashed curve with short intervals between the strokes) and gas and radiation pressure taken together (the solid curve) on the Rosseland mean of optical depth ($\log \tau_{\rm R}$). The horizontal lines show the magnetic pressure for magnetic strength B equal to 300 G (solid line) and 100 G (dashed line). The light–shaded area on the graph marks the area corresponding to Cyg X–1 optical component's photosphere. The dark–shaded area marks the area, corresponding to the stellar chromosphere.

5.2 Magnetic Field in Accretion Structure

The $\langle B_z \rangle$ derived from the He II emission line is located in the outer parts of the accretion structure (see above). Its value, ~ 600 G, is in agreement with Shvartsman's ideas (Kaplan & Shvartsman, 1976) that the gas stream carries the magnetic field to the accretion structure and the gas is compressed by a factor of ~ 10 due to an interaction with the structure of the outer rim. Along with an increase of gas density, the magnetic field is increased up to $B \sim 600$ G. It takes place at a distance of $6 \cdot 10^{11}$ cm $= 2 \cdot 10^5 R_g$ from the black hole (Bochkarev et al., 1975), where R_g is the gravitational radius. According to Shakura & Sunyaev (1973), we obtain $B \sim 10^9$ G at $3R_g$ for the standard model of the magnetized accretion disc. Taking into account the radiative pressure predominance within $\sim (10{-}20) R_g$, we obtain $B(3R_g) \sim (2{-}3) \cdot 10^8$ G. The measured value of the magnetic field strength at the marginal orbit of the Cyg X–1 black hole corresponds quite well with the Magnetic Coupling model with an equipartition between the kinetic and magnetic energy densities.

If the X–ray flickering is related to the magnetic nature, then the magnetic energy flux of the accreting matter must exceed the X–ray emission fluctuating component of luminosity. The region of the main energy release for the X-ray binaries extends from $5\,R_g$ to $27\,R_g$, and there should be a maximal frequency of $F \sim 100$ Hz for Cyg X–1 (see, e. g., Sunyaev & Revnivtsev, 2000). Inside the sphere of $27\,R_g$ radius the magnetic energy amounts to 10^{40} erg. The radial velocity of magnetized plasma at this radius in the Shakura–Sunyaev accretion disk is ~ 1.5 km/s (we adopt the viscosity parameter $\alpha = 1$ because the magnetic viscosity is large (Priest & Forbes, 2000; Tout & Pringle, 1992)). The time of matter infalling is ~ 1000 s. The magnetic energy flux is 10^{37} erg/s, which exceeds the flickering component power. Hence, magnetic energy dissipation permits to account for the X–ray flickering.

From the above–mentioned estimations the Cyg X–1 black hole magnetic moment is about 10^{30} G·cm^3. According to Robertson & Leiter (2003) such an object belongs to the Magnetic Extremely Compact Object (MECO) class.

5.3 Conclusions

Our main conclusions are as follows: we discovered a longitudinal magnetic field averaged over the picture plane $\langle B_z \rangle \sim 100\,\mathrm{G}$ in the photosphere of Cyg X–1 optical component. The real magnetic field can exceed $\langle B_z \rangle$. The magnetic field was detected at a high confidence level (about $6\,\sigma$) near the orbital phase $\varphi = 0.4$ in 2007, and $\varphi = 0.5$ in 2008. The dependence of $\langle B_z \rangle$ from φ is more complicated than that for a magnetic dipole, and probably varies within a year (Fig. 1). The magnetic field structure variability may be the reason of some long–term variations of the matter–flow process in this binary system.

Our results demonstrate that the 2007 – 2008 VLT FORS1 observations permit detecting the presence of a magnetic field in Cyg X–1. These are the pioneer measurements in a black hole system. The field can be responsible for the X–ray flickering. Our results indicate that it is necessary to take into account the impact of the magnetic field on the matter–flow structure in Cyg X–1.

Acknowledgements. We would like to acknowledge the ESO for granting the VLT observations in service mode. We thank V. V. Shimansky for his help in the stellar atmosphere model calculations. The work was partially supported by the RFBR grants 06–02–16843, 09–02–01136, 09–02–00993, 07–02–00535, and the grant of Support to Leading Scientific Schools of Russia 6110.2008.2.

References

Agafonov M. I., 2004, Radiophysics and Quantum Electronics, 47, No. 2, 85
Agafonov M. I., Richards M. T., Sharova O. I., 2006, ApJ, 652, 1547
Bagnulo S., Szeifert T., Wade G. A., Landstreet J. D., Mathys G., 2002, A&A, 389, 191
Bagnulo S., Landstreet J. D., Mason E., Andretta V., Silaj J., Wade G. A., 2006, A&A, 450, 777
Bochkarev N. G., Karitskaya E. A., Shakura N. I., 1975, Sov. Astr. Let., 1, 118
Bochkarev N. G., Karitskaia E. A., Siuniaev R. A., Shakura N. I., 1979, Sov. Astr. Let., 5, 99
Bochkarev N.G., Karitskaya E. A., Loskutov V. M., Sokolov V. V., 1986, Sov. Astron., 30, 43
Bochkarev N. G., Karitskaya E. A., 2011, in this volume
Boyarchuk A. A., Bisikalo D. V., Kuznetsov O. A., Chechetkin V. M., 2002, Advances in astronomy and astrophysics, v. 6, Taylor & Francis, London
Brocksopp C., Tarasov A. E., Lyuty V. M., Roche P., 1999, A&A, 343, 861
Dolan J. F., Tapia S., 1989, ApJ, 344, 830
Dolginov A. Z., Gnedin Yu. N., Silant'ev N. N., 1995, Propagation and polarization in cosmic media, Gordon & Breach Publ., Amsterdam
Gehrels T., 1972, ApJ, 173, L23
Gies D. R., Bolton C. T., Thomson J. R., Huang W., McSwain M. V., Riddle R. L., Wang Z., Wiita P. J., Wingert D. W.; Csák B., Kiss L. L., 2003, ApJ, 583, 424
Gnedin Yu. N., Borisov N. V., Natsvlishvili T. M., Piotrovich M. Yu., Silant'ev N. A., 2003, astro–ph/0304158
Gnedin Yu. N., Silant'ev N. A., Piotrovich M. Yu., Pogodin M. A., 2005, Astr. Rep., 49, 179
Hubrig S., Szeifert T., Schöller M., Mathys G., Kurtz D. W., 2004, A&A, 415, 685
Hubrig S., Schöller M., Schnerr R. S., González J. F., Ignace R., Henrichs H. F., 2008, A&A, 490, 793
Kaplan S. A. and Shvartsman V. F., 1976, "Origin and evolution of galaxies and stars", Nauka, Moscow, 319
Karitskaya E. A., 1981, Sov. Astron., 25, 80
Karitskaya E. A., 2007, in: Mashonkina L., Sachkov M. (eds), Conf. Proc., "Spectroscopical Methods in Modern Astrophysics", Moscow, 67
Karitskaya E. A., Agafonov M. I., Bochkarev N. G., Bondar A. V., Galazutdinov G. A., Lee B.–C., Musaev F. A., Sapar A. A., Sharova O. I., Shimanskii V. V., 2005, Astron. Astrophys. Transactions, 24, 383
Karitskaya E. A., Agafanov M. I., Bochkarev N. G., Bondar A. V., Galazutdinov G. A., Lee B.–C., Musaev F. A., Sharova O. I., Shimanskii V. V., Tarasov A. E., 2007a, Astron. Astrophys. Transactions, 26, 159
Karitskaya E. A., Bochkarev N. G., Bondar A. V., Galazutdinov G. A., Lee B.–C., Musaev F. A., Sapar A. A., Shimanskii V. V., 2008, Astronomy Reports, 52, 362

Karitskaya E. A., Bochkarev N. G., Hubrig S., Gnedin Yu. N., Pogodin M. A., Yudin R. V., Agafonov M. I., Sharova O. I., 2009, astro–ph0908.2719
Karitskaya E. A., Bochkarev N. G., Hubrig S., Gnedin Yu. N., Pogodin M. A., Yudin R. V., Agafonov M. I., Sharova O. I., 2010, IBVS, 5950, 1
Karitskaya E. A., Bochkarev N. G. et al., 2011, in: "Why Galaxies Care About AGB Stars. II", ASP Conf. Ser., (in press)
Karitskaya E. A., Shimanskii V. V., Sakhibullin N. A., Bochkarev N. G. 2007b, ASP Conf. Ser., 378, 123
Kemp J. C., Soutwick R. G., Rudy R. G., 1976, ApJ, 210, 235
Kemp J. C., 1980, A&A, 91, 108
Michalsky J. J., Swedlung J. B., 1977, ApJ, 212, 221
Nagae O., Kawabata K. S., Fukazawa Y., Okazaki A., Isogai M., 2009, AJ, 137, 3509
Priest E., Forbes T., 2000, MHD theory and applications, Cambridge University press
Pustilnik L. A., Shvartsman V. F., 1974, IAUS, 64, 213
Robertson S. L., Leiter D. J., 2003, ApJ, 45, L203
Shakura N. I., Sunyaev R. A., 1973, A&A, 24, 337
Shulov O. S., Kopatskaya E. N., 1972, Astron. Tsirk., 741, 5
Shvartsman V. F., 1971, Sov. Astron., 15, 377
Sunyaev R., Revnivtsev M., 2000, A&A, 358, 617
Tout C., Pringle J. E., 1992, MNRAS, 259, 604